# Micellar formation by soft template electropolymerization in organic solvents

Caroline Fradin, François Orange, Sonia Amigoni, Caroline R Szczepanski, Frédéric Guittard, Thierry Darmanin

## Graphical Abstract

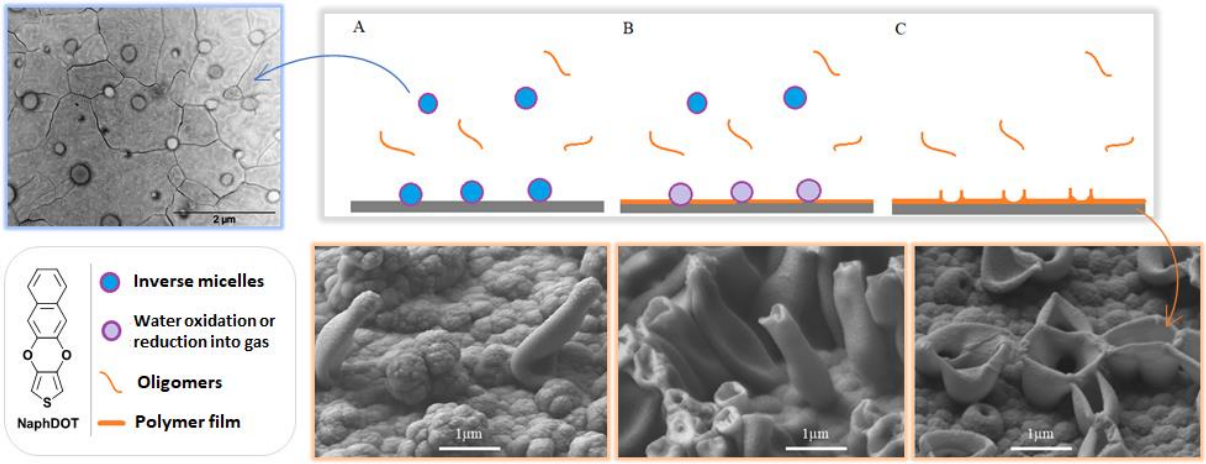


# Micellar formation by soft template electropolymerization in organic solvents

Caroline Fradin[a], François Orange[b], Sonia Amigoni[a], Caroline R. Szczepanski[c], Frédéric Guittard[a], and Thierry Darmanin[a,*]

[a]*Université Côte d'Azur, NICE Lab, 06100 Nice, France.*

[b]*Université Côte d'Azur, Centre Commun de Microscopie Appliquée (CCMA), 06100 Nice, France*

[c]*Michigan State University, College of Engineering, Dept. Chemical Engineering & Materials Science, MI 48824, Michigan, USA*

*Corresponding author:

NICE Lab
28 avenue Valrose
06100 Nice, France
Thierry.darmanin@unice.fr
06 34 12 10 13

**Abstract**

Hypothesis

The formation of porous nanostructures on surfaces and the control of their size and shape is fundamental for various applications. The creation of nanotubes is particularly difficult to implement without the aid of hard and rigid templates. Recently, methods that form nanotubular structures in a straightforward manner and without direct templating, e.g. soft templating, have been highly sought after. Here we propose the use of "soft templating" via self-assembly of conducting monomers during electropolymerization in organic solvents as a mean to form porous, nanotubular features.

Experiments

Naphtho[2,3-*b*]thieno[3,4-e][1,4]dioxine (NaphDOT) is employed as monomer for electropolymerizations conducted in dichloromethane and chloroform containing varying amounts of water. SEM analyses of the resulting surfaces confirms the strong capacity of NaphDOT to form vertically aligned nanotubes. Polymerization solutions analyzed by DLS and TEM reveal the presence of micelles prior to electropolymerization, and the size of the micelles correlates with the inner diameter of the nanotubes formed.

Findings

We show that micelles in polymerization solutions are stabilized by both monomers and electrolytes. We propose a mechanism where reverse micelles are forming a soft-template responsible for the formation of porous nanostructures during electropolymerization in organic, non-polar solvents. In this mechanism, the monomer and electrolyte assume the role of surfactant in the reverse micelle system.

**Keywords:** electropolymerization, soft-template, reverse micelles, porous nanostructures.

## 1. Introduction

The design of nanostructures such as nanotubes on surfaces is fundamental for several applications including sensors, photocatalysis, magnetism, energy storage, optical and electronic devices and also for tuning surface wettability [1–7]. In that last case, nanotubes often

impart superhydrophobic properties to a surface. The amount of air trapped within the nanotubes acts directly on the adhesion of water droplets on the surface. Thereby their geometry can impart unique adhesive behaviors between water droplets and the surface, sometimes resulting in strong hydrophobicity and adhesion [7].

An efficient approach to build nanotubes is through polymerization on a hard template [8,9]. Previously, electropolymerization of conductive polymers (e.g., polypyrrole, poly(3,4-ethylenedioxythiophene (PEDOT)) has been employed to form nanotubes with this approach [10,11]. Unfortunately, this strategy comes with disadvantages, most importantly that it is quite labor- and material-intensive; the templates are often single-use and therefore a totally new template is required to manipulate or adjust a single nanotube parameter (e.g., height, diameter, etc.).

To avoid these limitations, nanotubes can also be obtained by employing templateless electropolymerization. For example, nanotubes are formed during the electropolymerization of pyrrole without any hard template. During electropolymerization, the water ($H_2O$) used as solvent is oxidized or reduced into $O_2$ or $H_2$, creating gas bubbles that can be stabilized on the substrate by surfactants included in the aqueous monomer solution, such as camphorsulfonic acid [12] or *beta*-naphtalene sulfonic acid [13–17]. Being stabilized, the gas bubbles act as a soft template for electropolymerization. Another approach to develop polypyrrole nanotubes has been described, however instead of surfactant, weak acid anions (such as inorganic chlorate or phosphate salts) are employed [18–22]. In this case, the presence of weak acid anions inhibits the oxidation of pyrrole, enhancing water oxidation. This over-oxidizes the polypyrrole layer, making it insulating except for discrete sites that are protected by $O_2$ bubbles. When pyrrole electropolymerization starts again, it proceeds on the protected, discrete sites and leads to the formation of nanotubes. With this mechanism, the over-oxidation of polypyrrole generates the soft template during electropolymerization.

While the prior examples were isolated to aqueous systems, soft template electropolymerizations can also be performed in organic solvents, particularly dichloromethane ($CH_2Cl_2$), and with various conductive monomers including thiophene-based derivatives [23–28]. The suggested mechanism for nanostructure formation in organic solvents relies on the generation of gas bubbles by trace water oxidation or reduction. The gas bubbles are then stabilized on electrode surfaces by monomers and/or electrolytes that act as surfactants. However, up to now, the only evidence of this mechanism is the presence of the water reduction peak observed on voltammograms, even in anhydrous solvents, as well as the resulting porous structures on the polymer surfaces [29,30].

In this study we demonstrate, for the first time, that in electropolymerization solutions, reverse aqueous micelles stabilized by monomer and electrolytes form prior to the onset of polymerizations. Moreover, we also demonstrate that the size of these micelles correlates with the inner diameter of nanotubes that form via subsequent electropolymerization. For this study, naphtho[2,3-*b*]thieno[3,4-e][1,4]dioxine (NaphDOT) was chosen as monomer for all electropolymerizations, due to its previously demonstrated strong capacity to form nanotubular structures, even at very low $H_2O$ content (**Scheme 1**) [31, 32]. Dichloromethane ($CH_2Cl_2$) and chloroform ($CHCl_3$) were chosen as organic solvents and were saturated with $H_2O$ to determine the influence of $H_2O$ content on the formation of micelles prior electropolymerization, as well as the resulting surface structures.

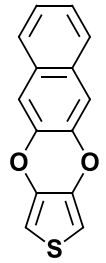

NaphDOT

**Scheme 1.** Monomer studied in this manuscript.

## 2. Experimental Section

### 2.1. Electropolymerization parameters

The monomer, NaphDOT, was synthesized according to previous works [32,33] and polymerized via electrodeposition onto gold plates. Electrodepositions were performed with an Autolab potentiostat of Metrohm (Autolab) using a three-electrode system: a gold plate as working electrode, a carbon rod as counter-electrode and a saturated calomel electrode (SCE) as reference electrode. For all electropolymerizations, a solution of 0.1 M tetrabutylammonium perchlorate ($Bu_4NClO_4$) and 0.01 M of monomer was used. The solvents employed included anhydrous $CH_2Cl_2$ or $CHCl_3$, as well as either of these saturated with water, (referred throughout the text as: $CH_2Cl_2$ + $H_2O$ sat. and $CHCl_3$ + $H_2O$ sat.). Saturated solvents were prepared by mixing the organic solvent with a large amount of water and collecting the organic phase. An intermediate water content of the solvents ($H_2O$ 50% sat.) was prepared by diluting by half (in volume) $CH_2Cl_2$ + $H_2O$ sat. or $CHCl_3$ + $H_2O$ sat. with anhydrous analogues. In order to release a large number of gas bubbles, electrodepositions were performed via cyclic

voltammetry, from -1 V to the monomer oxidation potential ($E^{ox}$ = 1.80 V vs SCE for NaphDOT) and at a scan rate of 20 mV $s^{-1}$.

### 2.2. Micelle characterization

Sizes of the micelles were determined via dynamic light scattering using a Vasco γ Particle Size Analyzer (Cordouan Technologies) and the software NanoQ V2.5.5.0. The sizes presented are the average of 3 different experiments of 6 measurements each.

Electropolymerization solutions were observed by transmission electron microscopy (TEM) prior to electrodeposition and also after 5 cyclic voltammetry scans using a JEOL JEM-1400 TEM. The solution compositions are the same as described above. For imaging, a drop of 0.45 µm-filtered solution was deposited onto a 400 mesh TEM copper grid with a carbon support film and the exceeding liquid was absorbed with a paper filter to avoid excessive salt deposition onto the TEM grids.

Size measurements on TEM and MEB pictures were performed using ImageJ. Population distributions were calculated with at least 170 subjects. The mean sizes and standard deviations were calculated fitting the distribution with a gaussian model using the least square method.

### 2.3. Surface characterization

Surface morphology was evaluated via scanning electron microscopy (SEM) using a JEOL 6700F SEM after platinum coating. Static water contact angles of the polymer films were measured using a DSA30 goniometer of Bruker and determined via the sessile-drop method with 2µL water droplets.

## 3. Results and Discussion

### 3.1. Micelle characterization

Diffusion Light Scattering (DLS) measurements were performed with solutions of NaphDOT monomers and $Bu_4NClO_4$ containing $CHCl_3$ or $CHCl_3$ + $H_2O$ sat. as solvent. The DLS measurements revealed bimodal distributions of sizes for samples containing NaphDOT and $Bu_4NClO_4$ (C and C'), as well as those containing only $Bu_4NClO_4$ (B and B'). The mean

size of each mode is reported in **Table 1**. The sizes of the objects do not depend on the water content of the solvent, as no significant difference is observed for the water saturated solvents. No objects were detected in the solutions containing only solvents (A and A'). Several size distributions were observed for solution D that underwent 5 cyclic voltammetry electropolymerizations. This different size distributions are likely suspended oligomers, which explains the difference compared to samples B and C.

**Table 1**. Micelle size measurements of solutions with concentrations used in the electropolymerization process. The first two columns highlight the DLS results (means of distribution modes) and the last columns contain the micelles mean sizes and standard deviations calculated by a gaussian fit on the diameter distributions measured on TEM images, as well as the surfaces structures diameter observed by MEB, respectively.

| Sample | | DLS First mode (nm) | DLS Second mode (nm) | TEM micellar size distribution | MEB Nanostructures diameter (nm) |
|---|---|---|---|---|---|
| A | $CHCl_3$ | | | | |
| A' | $CHCl_3$ + $H_2O$ sat. | | | | |
| B | $Bu_4NClO_4$ + $CHCl_3$ | 34 ± 4 | 773 ± 354 | | |
| B' | $Bu_4NClO_4$ + $CHCl_3$ + $H_2O$ sat. | 25 ± 3 | 655 ± 347 | | |
| C | NaphDOT + $Bu_4NClO_4$ + $CHCl_3$ | 16 ± 3 | 151 ± 4 | 84 ± 25<br>291 ± 83 | Outer 334 ± 39 |
| C' | NaphDOT + $Bu_4NClO_4$ + $CHCl_3$ + $H_2O$ sat. | 32 ± 6 | 181 ± 51 | 166 ± 57 | Outer 399 ± 42 nm<br>Inner 151 ± 46 nm |
| D | NaphDOT + $Bu_4NClO_4$ + $CHCl_3$ **(5 scans)** | 10 ± 1<br>30 ± 8 | 184 ± 53<br>521 ± 66 | 89 ± 30<br>201 ± 47 | |
| D' | NaphDOT + $Bu_4NClO_4$ + $CHCl_3$ + $H_2O$ sat. (**5 scans)** | 12 ± 2 | 539 ± 103 | 220 ± 66 | |

TEM observations of solutions B, B', C, C', D, and D' (**Fig. 1**) confirmed the presence of micelles, even in the solutions without any NaphDOT monomers (B, B'). The diameters of the micelles were measured on random TEM images. In samples containing water in the solvent (C' and D'), the micellar distributions are mono-modal (**Fig. 1**) with a bigger mean size observed for sample D' (237 ± 92 nm) than C' (174 ± 66 nm). With D', the reverse micelles grew

during the electropolymerization of this solution, which is supported by the appearance of oligomers in solution. The first distribution mode detected by the DLS was not observed in the TEM images so its existence is not confirmed. The TEM images gives more precise sizes than DLS but objects smaller than 50 nm cannot be detected.

Micellar distributions observed in TEM images were bimodal in samples containing anhydrous solvent (C and D), see **Fig. 1**. The size of their second mode is similar to the size of the reverse micelles measured on TEM images for samples C' and D' (200-300nm). Since anhydrous solvents still contain trace amounts of water, that are often visible on cyclic voltammetry curves [29,30], these larger micelles are surely reverse micelles and the smaller ones with approximate size of 80 nm are micelles formed by the electrolytes and monomers only. These results highlighting variations in number of reverse micelles but not their size as a function of water content correlate with a prior study focused on a different monomer, where it was demonstrated that increasing water content increases the overall number of nanotubes but not their size [29].

TEM images of samples B and B' also showed two populations of micelles, following the DLS results. Their nature is here different because of the absence of monomers, the smaller micelles being electrolytes aggregates and the bigger reverse micelles, and therefore their sizes are not reported in Table 1.

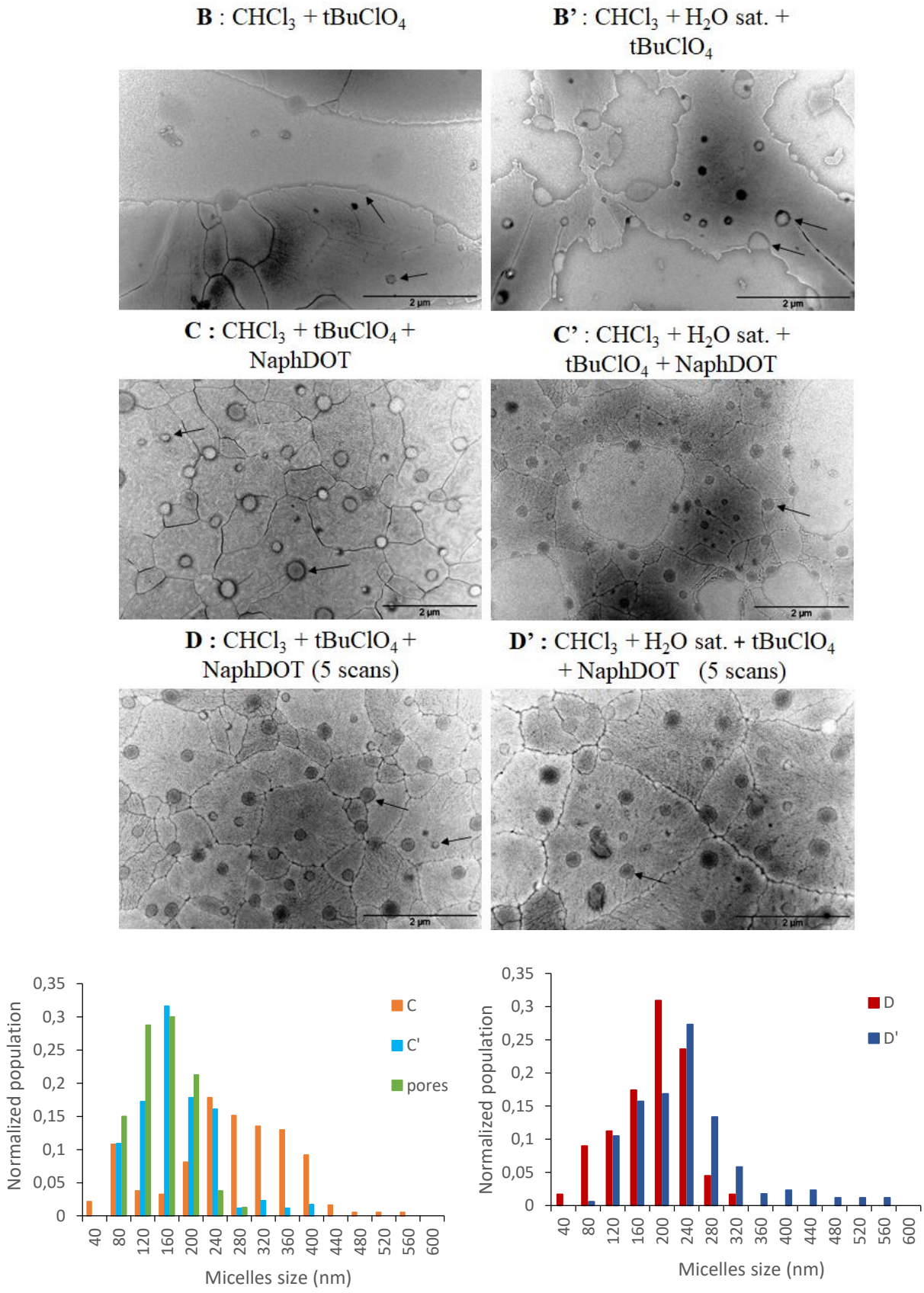


**Figure 1.** Upper panel: TEM observations of monomer solutions in $CHCl_3$ before and after polymerization. (scale bars are 2µm in each image). Lower panel: Micellar sizes distributions

of solutions D (red) and D' (dark blue), C (orange) and C'(light blue) measured on TEM images and pores diameters distribution (green) of NaphDOT film (3 cyclic voltammetry scans in $CHCl_3$ + $H_2O$ sat.) measured on SEM images.

### 3.2. Characterization of the nanoporous polymer films

In order to confirm that the reverse micelles lead to the formation of nanostructures during electropolymerization, all surfaces were characterized by SEM (with and without substrate inclination) to estimate the size of surface structures (**Figure 2**).

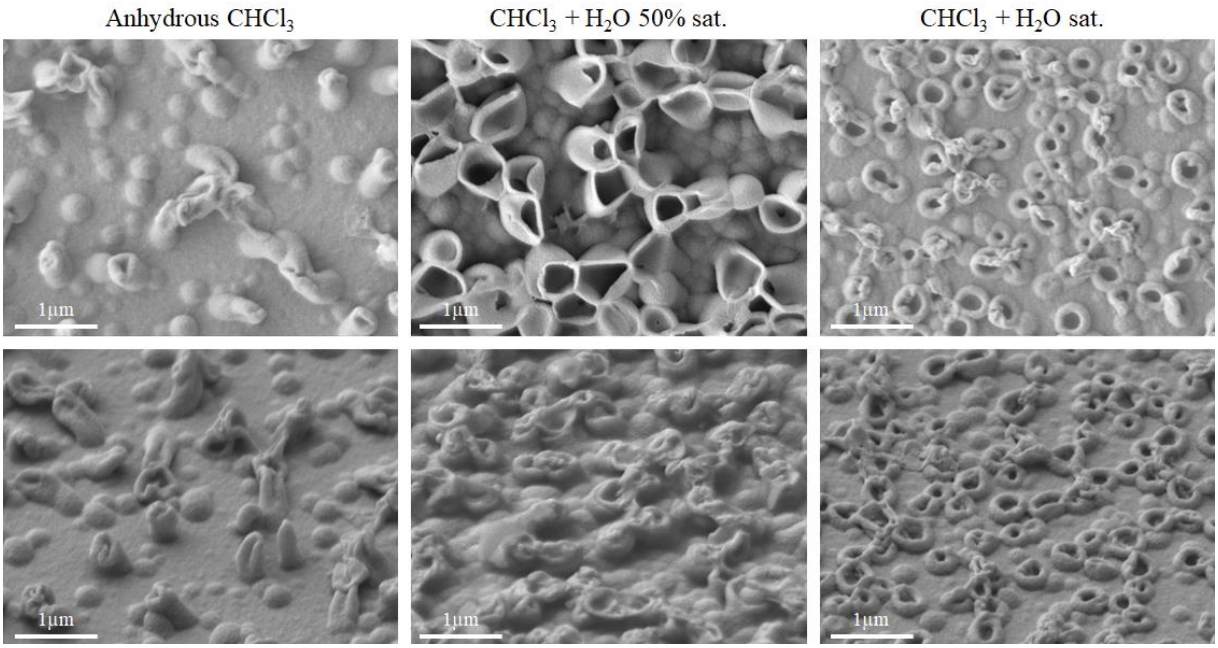


**Figure 2.** SEM observations of NaphDOT after 3 cyclic voltammetry scans in $CHCl_3$, with varying water content. Both horizontal images (top row) and inclined images (bottom row) are displayed.

In anhydrous $CHCl_3$, NaphDOT electropolymerization formed some nanotubules, however they are not very porous (**Fig. 2**, left column). However, with $CHCl_3$ + $H_2O$ sat. as solvent, many nanorings are clearly observed on the surface (**Fig. 2,** right column). The increase in water content has two effects: (1) it increases the number of tubes, and (2) it slightly decreases their size, which is expected if the same amount of polymer is deposited. The hydrophobicity of the films also decreases with increasing the water content of the solvent ($\theta_w$=124 ± 8°, 91 ± 5° and 87 ± 7° respectively).

The sizes of the surface nanostructures were measured in the SEM images taken of surfaces after 3 cyclic voltammetry scans. In $CHCl_3$, the mean outer diameter of the nanostructures was **334 ± 39 nm**, which is slightly larger than the micelle size observed in TEM images or measured via DLS (sample C, **Table 1**). This makes sense since the size measured via SEM is the outer diameter of the structure. In $CHCl_3$ + $H_2O$ sat., the mean outer-diameter of the nanorings was similar (**399 ± 42 nm).** However, in this case it was also feasible to measure the inner-diameter of the different nanorings, revealing an average size of **151 ± 46 nm.** This corresponds perfectly with the reverse micelle size of sample C' (**Fig. 1**).

This last result proves that the observed micelles, once adsorbed onto the electrode surface, can serve as a soft template for NaphDOT polymerization (**Scheme 2**). Once adsorbed, the water contained in the micelles is either oxidized or reduced to $O_2$ or $H_2$ gas, and the gas is eventually released leading to porous nanostructures. If the polymer growth proceeds in a unidimensional fashion, depending on the molecular interactions, nanotubes are formed.

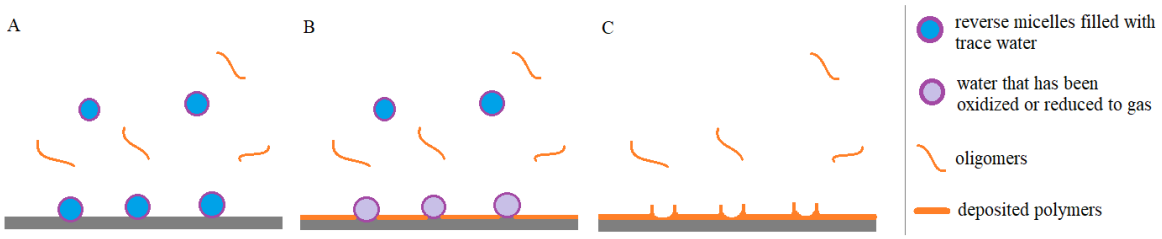


**Scheme 2.** Proposed mechanism. **A**. Reverse micelles are adsorbed on the substrate. **B.** Micelles act as a soft-template for polymer deposition and water is oxidized or reduced inside the micelles. **C.** Gas bubbles are released and polymer growth continues.

### 3.3. Role of the monomer in the micelle stabilization

Since micelles are also present in solutions without NaphDOT monomer (B and B'), we tried to determine the role of the monomer in the formation of such micelles. DLS experiments were performed with different NaphDOT concentrations in the solutions, yet fixed electrolyte concentration of 100 mM (**Figure 3**). The size of the micelles appears to increase with the quantity of NaphDOT in solution, showing that the monomer takes part in the formation of reverse micelles. Therefore, the electrolytes and monomers are acting as co-surfactants. At the electropolymerization concentration (10mM) (which corresponds to samples C and C'), a second group of smaller micelles are also detected, which are likely aggregates of NaphDOT monomers and electrolytes. Samples in anhydrous $CHCl_3$ showed exactly same results as those in $CHCl_3$ + $H_2O$ sat, revealing that water content does not significantly alter micelle size.

**Figure 3** shows SEM images of surfaces after NaphDOT electrodeposition in $CHCl_3$ with varying water content, and monomer concentrations of 5 and 10 mM. The overall morphology of the structures does not change significantly, however the diameter of the nanorings decreases with decreasing monomer concentration. This result is in agreement with the DLS experiments which indicated that micelle size decreased with monomer concentration.

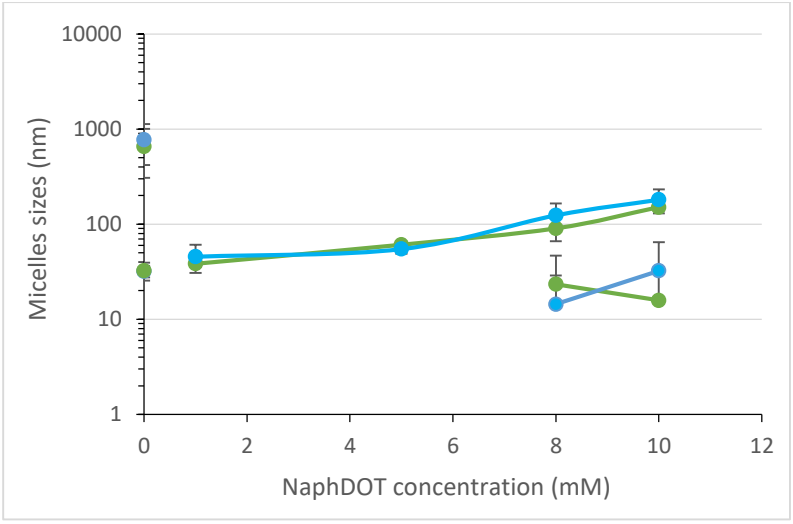


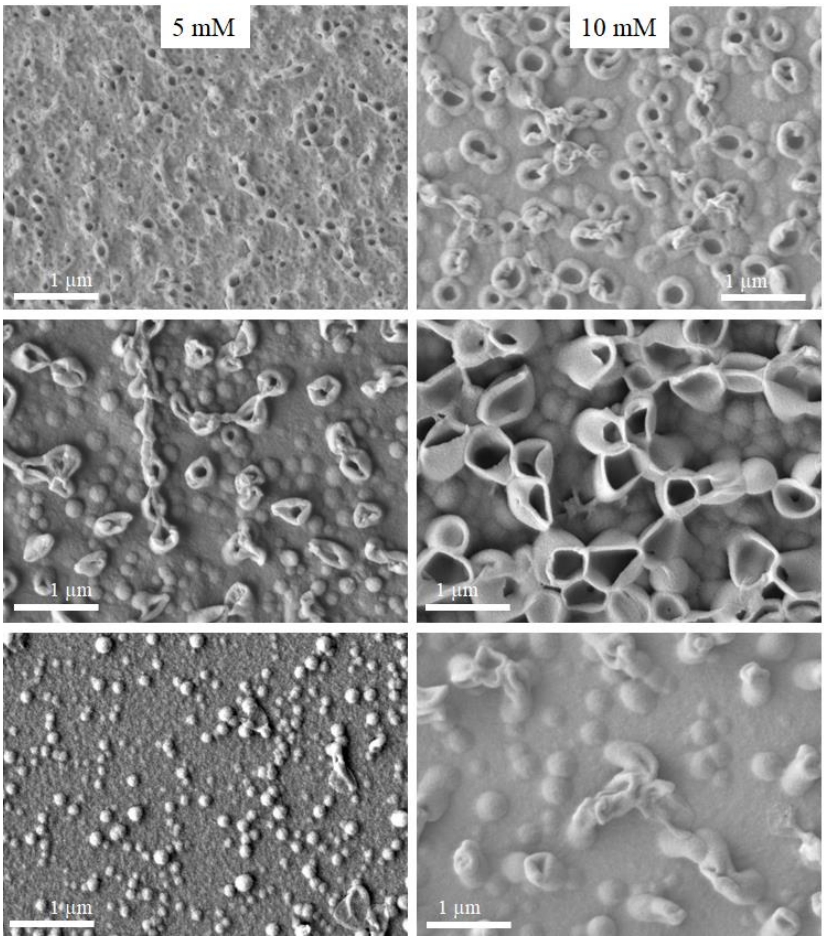


$CHCl_3$ + $H_2O$ sat.

$CHCl_3$ + $H_2O$ 50% sat.

Anhydrous $CHCl_3$

**Figure 3.** Upper panel: DLS results for solutions with 100mM $Bu_4NClO_4$ and two different NaphDOT concentrations. Blue: $CHCl_3$ + $H_2O$ sat. and green: anhydrous $CHCl_3$. Lower panel: SEM observations (x25000) of NaphDOT 3 cyclic voltammetry scans depositions in chloroform with different amount of water and monomers concentration.

With the existence of micelles stabilized by NaphDOT monomers and electrolytes being demonstrated in chloroform, and the role of these micelles as soft-templates for porous electrodeposited films, we also wonder if this mechanism is possible in other solvents.

### 3.4. Generalization to electropolymerization in others organic solvents

In addition to $CHCl_3$, the NaphDOT monomer is well known for its strong capacity to form vertically aligned nanotubes when electropolymerized in $CH_2Cl_2$ [31,32]. To determine the influence of $H_2O$ content on the surface structures when polymerized in $CH_2Cl_2$, NaphDOT was electropolymerized in $CH_2Cl_2$ + $H_2O$ sat. and $CH_2Cl_2$ + $H_2O$ 50% sat. The SEM images (**Figure 4**) from these experiments reveal that the number of tubes formed from electrodeposition again increases with water content. This is consistent with the proposed mechanism (**Scheme 2**). Furthermore, the tubes are more open with increased water content, and with $CH_2Cl_2$ + $H_2O$ sat., the tubes are larger and shorter, with walls folded up. As in $CHCl_3$, the structures become more porous with increasing water content, but the tubes have visibly smaller diameters with electropolymerization in $CHCl_3$ than in $CH_2Cl_2$, leading to a higher hydrophobicity of the films ($\theta_w$=121 ± 5°, 144 ± 2° and 93 ± 6° for surfaces polymerized in $CH_2Cl_2$ with increasing water content). TEM observations of NaphDOT solutions with $Bu_4NClO_4$ in $CH_2Cl_2$ confirmed the presence of micelles, however of a larger size (around 500 nm). This difference in micelle size between the two solvents can be related to the higher solubility of $H_2O$ in $CH_2Cl_2$ (123mM) [34] than in $CHCl_3$ (73mM) [35]. If more water is solubilized in $CH_2Cl_2$ than compared to $CHCl_3$, the micelle size should be bigger, and thus the gas bubbles and resulting nanotubes.

This can also explain why NaphDOT electropolymerization in acetonitrile [32] did not form porous structures. Acetonitrile is indeed a polar solvent ($\mu$= 3,45 D) that is miscible with water, and its non-dissociating properties ($\varepsilon_r$ = 37,5) prevent electrolytes from stabilizing potential micelles. DLS measurements of $Bu_4NClO_4$ solutions in acetonitrile confirmed the non-existence of such reverse micelles.

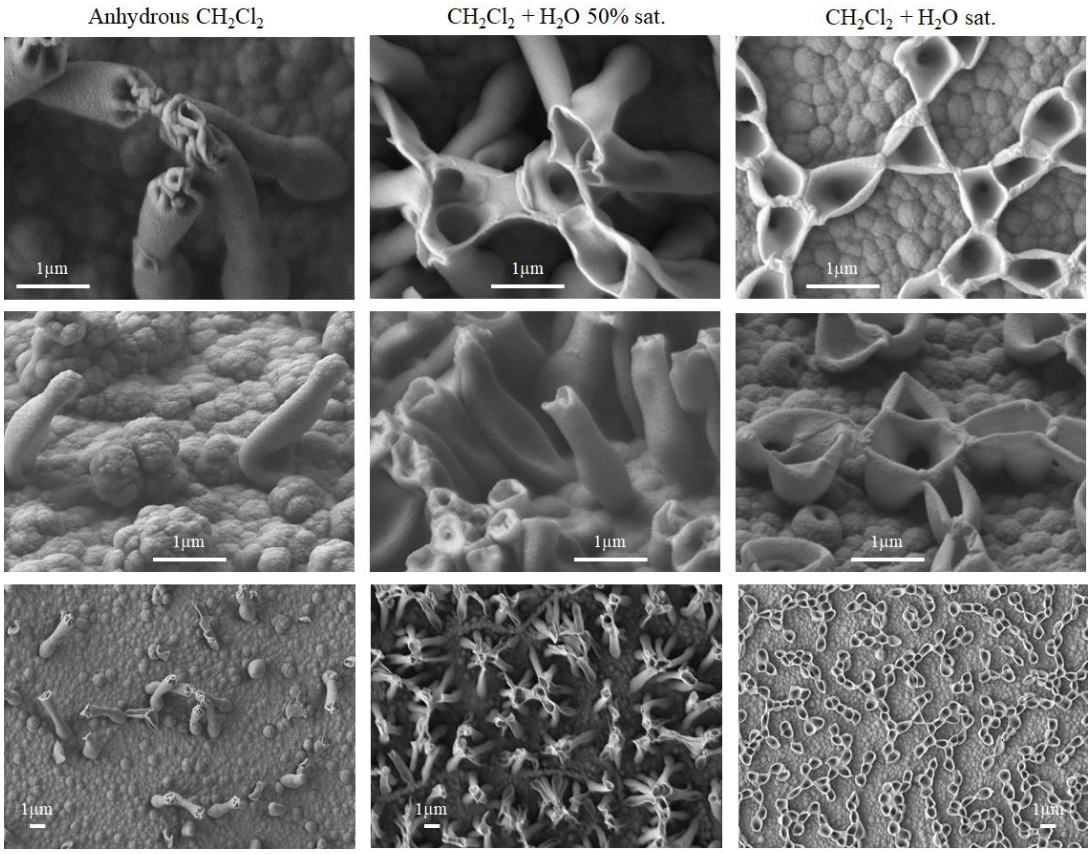


**Figure 4.** SEM observations of NaphDOT cyclic voltammetry scans depositions in $CH_2Cl_2$ with various water content, flat (first row) and inclined (second row) pictures at a tiny scale and at a larger scale (bottom row).

## 4. Conclusion

Electropolymerization is a very convenient technique to obtain surfaces with porous nanostructures like nanotubes that are used in many applications such as water harvesting, sensors, catalysis and water/oil separation [1-7]. A better knowledge of the mechanism leading to porous nanostructures will enable a finer control of the nanostructures and a focus on relevant monomers for this surface design. In this study, we demonstrated for the first time that the formation of porous nanostructures by electropolymerization in organic solvents of low polarity such as chloroform and dichloromethane is due to the presence of reverse micelles in solution prior to the onset of polymerization.

Based on previous works on electropolymerization in water using a surfactant [12-17], this work demonstrated that the micelles observed in organic solvent are stabilized by monomers and electrolytes playing the role of a surfactant. Once adsorbed onto the electrode,

they act as a soft template for polymer electrodeposition. The water inside the micelle is oxidized or reduced, forming gases that are released during the electrodeposition. With an increasing amount of water in a solvent, the number of micelles increases but not their size, leading to a surface with more densely packed nanostructures. This corresponds with observations previously reported in the literature [29, 30].

Further investigations are necessary to determine the role of the electrolytes on the stabilization of the reverse micelles and how to extend this behavior to other monomers.

## 5. Acknowledgement

The authors would like to acknowledge *Agence Innovation Défense* for their grant and support. This work has been supported by CNRS GDR 2088 « BIOMIM ».

## 6. Author contributions

Caroline Fradin performed the experiments and François Orange carried out MET observations. Sonia Amigoni, Caroline Fradin and Thierry Darmanin contributed to the interpretation of the results. Caroline Fradin, Caroline R. Szczepanski and Thierry Darmanin wrote the manuscript with input of all authors. Frederic Guittard supervised the project.

## References

[1] K.R. Park, H.B. Cho, J. Lee, Y. Song, W.B. Kim, Y.H. Choa, Design of highly porous $SnO_2$-CuO nanotubes for enhancing $H_2S$ gas sensor performance, Sens. Actuators B Chem. 302 (2020) 127179.

[2] G. He, J. Zhang, Y. Hu, Z. Bai, C. Wei, Dual-template synthesis of mesoporous $TiO_2$ nanotubes with structure-enhanced functional photocatalytic performance, Appl. Catal. B 250 (2019) 301–312.

[3] R.J. Martín-Palma, P.D. McAtee, R. Ramadan, A. Lakhtakia, Hybrid nanostructured porous silicon-silver layers for wideband optical absorption, Sci. Rep. 9 (2019) 7291.

[4] A. Marmur, Hydro- hygro- oleo- omni-phobic ? Terminology of wettability classification, Soft Matter 8 (2012) 6867–6870.

[5] T. Darmanin, F. Guittard, Superhydrophobic and superoleophobic properties in Nature, Mater. Today 18 (2015) 273−285.

[6] S. Yu, Z. Guo, W. Liu, Biomimetic transparent and superhydrophobic coatings: From nature and beyond nature, Chem. Commun. 51 (2015) 1775−1794.

[7] Z. Cheng, J. Gao, L. Jiang, Tip geometry controls adhesive states of superhydrophobic surfaces, Langmuir 26 (2010) 8233−8238.

[8] Y. Cheng, H. Yang, Y. Yang, J. Huang, K. Wu, Z. Chen, X. Wang, C. Lin, Y. Lai, Progress in $TiO_2$ nanotube coatings for biomedical applications: A review, J. Mater. Chem. B 6 (2018) 1862−1886.

[9] H.-A. Lin, S.-C. Luo, B. Zhu, C. Chen, Y. Yamashita, H.-h. Yu, Molecular or nanoscale structures? The deciding factor of surface properties on functionalized poly(3,4ethylenedioxythiophene) nanorod arrays, Adv. Funct. Mater. 23 (2013) 3212–3219.

[10] S. Demoustier-Champagne, P.Y. Stavaux, Effect of electrolyte concentration and nature on the morphology and the electrical properties of electropolymerized polypyrrole nanotubules, Chem. Mater. 11 (1999) 829–834.

[11] R. Xiao, S.I. Cho, R. Liu, S.B. Lee, Controlled electrochemical synthesis of conductive polymer nanotube structures, J. Am. Chem. Soc. 129 (2007) 4483–4489.

[12] L. Qu, G. Shi, J. Yuan, G. Han, F. Chen, Preparation of polypyrrole microstructures by direct electrochemical oxidation of pyrrole in an aqueous solution of camphorsulfonic acid, J. Electroanal. Chem. 561 (2004) 149–156.

[13] L. Qu, G. Shi, F. Chen, J. Zhang, Electrochemical growth of polypyrrole microcontainers, Macromolecules 36 (2003) 1063–1067.

[14] S. Gupta, Hydrogen bubble-assisted syntheses of polypyrrole micro/nanostructures using electrochemistry: structural and physical property characterization, J. Raman Spectrosc. 39 (2008) 1343–1355.

[15] J.T. Kim, S.K. Seol, J.H. Je, Y. Hwu, G. Margaritondo, The microcontainer shape in electropolymerization on bubbles, Appl. Phys. Lett. 94 (2009) 034103.

[16] B. Parakhonskiy, D. Andreeva, H. Möhwald, D.G. Shchukin, Hollow polypyrrole containers with regulated uptake/release properties, Langmuir 25 (2009) 4780–4786.

[17] B. Parakhonskiy, D.G. Shchukin, Polypyrrole microcontainers: Electrochemical synthesis and characterization, Langmuir 31 (2015) 9214–9218.

[18] C. Debiemme-Chouvy, One-step electrochemical synthesis of a very thin overoxidized polypyrrole film, Electrochem. Solid-State Lett. 10 (2007) E24–E26.

[19] A. Fakhry, F. Pillier, C. Debiemme-Chouvy, Templateless electrogeneration of polypyrrole nanostructures: impact of the anionic composition and pH of the monomer solution, J. Mater. Chem. A 2 (2014) 9859–9865.

[20] C. Debiemme-Chouvy, Template-free one-step electrochemical formation of polypyrrole nanowire array, Electrochem. Commun. 11 (2009) 998–301.

[21] A. Fakhry, H. Cachet, C. Debiemme-Chouvy, Mechanism of formation of templateless electrogenerated polypyrrole nanostructures, Electrochim. Acta 179 (2015) 297–303.

[22] A. Turco, E. Mazzotta, C. Di Franco, M.V. Santacroce, G. Scamarcio, A.G. Monteduro, E. Primiceri, C. Malitesta, Templateless synthesis of polypyrrole nanowires by non-static solution-surface electropolymerization, J. Solid State Electrochem. 20 (2016) 2143–2151.

[23] S. Bai, Q. Hu, Q. Zeng, M. Wang, L. Wang, Variations in surface morphologies, properties, and electrochemical responses to nitro-analyte by controlled electropolymerization of thiophene derivatives, ACS Appl. Mater. Interfaces 10 (2018) 11319–11327.

[24] Y. Huang, S. Bai, H. Jianzhi, M. Ya, Q. Zeng, M. Wang, L. Wang, Simultaneous detection of nitrophenol isomers using an easy-to-fabricate thiophene-based microporous polymer film modified electrode, Microchem. J. 153 (2020) 104465.

[25] S.-C. Luo, J. Sekine, B. Zhu, H. Zhao, A. Nakao, H.-h. Yu, Polydioxythiophene nanodots, nonowires, nano-networks, and tubular sructures: The effect of functional groups and temperature in template-free electropolymerization, ACS Nano 6 (2012) 3018–3026.

[26] O. Sane, A. Diouf, G. Moran Cruz, F. Savina, R. Méallet-Renault, S. Amigoni, S.Y. Dieng, F. Guittard, T. Darmanin, Coral-like nanostructures, Mater. Today 31 (2019) 119–120.

[27] T. Darmanin, E.L. Klimareva, I. Schewtschenko, F. Guittard, I.F. Perepichka, Exceptionally strong effect of small structural variations in functionalized 3,4-phenylenedioxythiophenes on the surface nanostructure and parahydrophobic properties of their electropolymerized films, Macromolecules 52 (2019) 8088–8102.

[28] C. Fradin, F. Guittard, T. Darmanin, A soft template approach to various porous nanostructures from conjugated carbazole-based monomers, J. Colloid Interface Sci. (2020) DOI: 10.1016/j.jcis.2020.10.010.

[29] E.h.Y. Thiam, A. Dramé, S. Sow, A. Sene, C.R. Szczepanski, S.Y. Dieng, F. Guittard, T. Darmanin, Designing nanoporous membranes through templateless electropolymerization of thieno[3,4-b]thiophene derivatives with high water content, ACS Omega 4 (2019) 13080−13085.

[30] S. Sow, F. Sow, A. Dramé, F. Orange, A. Sene, S.Y. Dieng, F. Guittard, T. Darmanin, Influence of alkyl spacer in nanostructure shape control by templateless electropolymerization, Prog. Org. Coat. 138 (2020) 1053822.

[31] T. Darmanin, F. Guittard, A one-step electrodeposition of homogeneous and vertically aligned nanotubes with parahydrophobic properties (high water adhesion), J. Mater. Chem. A 4 (2016) 3197–3203.

[32] T. Darmanin, J.-P. Laugier, F. Orange, F. Guittard, Influence of the monomer structure and electrochemical parameters on the formation of nanotubes with parahydrophobic properties (high water adhesion) by a templateless electropolymerization process, J. Colloid Interface Sci. 466 (2016) 413–424.

[33] E. Poverenov, Y. Sheynin, N. Zamoshchik, A. Patra, G. Leitus, I.F. Perepichka, M. Bendikov, Flat conjugated polymers combining a relatively low HOMO energy level and band gap: Polyselenophenes versus polythiophenes, J. Mater. Chem. 22 (2012) 14645–14655.

[34] W. Davis, J.B. Jagger, H.K. Whalley, Methylene dichloride and 1,2-dichloroethane. I. Solubility of water. II. Vapour pressure, J. Soc. Chem. Ind. 68 (1949) 26–31.

[35] J. Kirchnerova, G.B. Cave, The solubility of water in low-dielectric solvents, Can. J. Chem. 54 (1976) 3909–3916.

## Figures captions

**Scheme 1.** Monomer studied in this manuscript.

**Scheme 2.** Proposed mechanism. **A**. Reverse micelles are adsorbed on the substrate. **B.** Micelles act as a soft-template for polymer deposition and water is oxidized or reduced inside the micelles. **C.** Gas bubbles are released and polymer growth continues.

**Figure 1.** Upper panel: TEM observations of monomer solutions in $CHCl_3$ before and after polymerization. (scale bars are 2µm in each image). Lower panel: Micellar sizes distributions of solutions D (red) and D' (dark blue), C (orange) and C'(light blue) measured on TEM images and pores diameters distribution (green) of NaphDOT film (3 cyclic voltammetry scans in $CHCl_3$ + $H_2O$ sat.) measured on SEM images.

**Figure 2.** SEM observations of NaphDOT after 3 cyclic voltammetry scans in $CHCl_3$, with varying water content. Both horizontal images (top row) and inclined images (bottom row) are displayed.

**Figure 3.** Upper panel: DLS results for solutions with 100mM $Bu_4NClO_4$ and two different NaphDOT concentrations. Blue: $CHCl_3$ + $H_2O$ sat. and green: anhydrous $CHCl_3$. Lower panel: SEM observations (x25000) of NaphDOT 3 cyclic voltammetry scans depositions in chloroform with different amount of water and monomers concentration.

**Figure 4.** SEM observations of NaphDOT cyclic voltammetry scans depositions in $CH_2Cl_2$ with various water content, flat (first row) and inclined (second row) pictures at a tiny scale and at a larger scale (bottom row).

**Table 1**. Micelle size measurements of solutions with concentrations used in the electropolymerization process. The first two columns highlight the DLS results (means of distribution modes) and the last columns contain the micelles mean sizes and standard deviations calculated by a gaussian fit on the diameter distributions measured on TEM images, as well as the surfaces structures diameter observed by MEB, respectively.